Grain Crushing under Pile Tip Explored by Acoustic Emission

Wuwei Mao[1], Ikuo Towhata[2], Shogo Aoyama[3] and Shigeru Goto[4]
[1]*Department of Civil Engineering, University of Tokyo, Tokyo, Japan*
[2]*Visiting professor, Kanto Gakuin University, Yokohama, Japan*
[3]*Kiso - Jiban Consultants Co., Ltd., Tokyo, Japan*
[4]*Faculty of Science and Engineering, Waseda University, Tokyo, Japan*
[2]*E-mail:* towhata.ikuo.ikuo@gmail.com

ABSTRACT: Recent practice in design of pile foundations under vertical load relies significantly on either a classic plasticity framework or empiricism. Despite efforts to explore the real pile behavior mainly in 1960s and 1970s, research interest has decreased in the recent times. Accordingly, much is not known about the group pile behavior that is more complicated than that of a single pile. One of the possible reasons for this poor situation is the lack of novel research methodology. In this regard, the authors chose the behavior of both a single pile and group piles subjected to vertical load, and carried out model tests using several new research tools. One important finding was the significant vertical compression of sand under the pile tips which was accompanied by crushing of sand grains. To further investigate the process of grain crushing, the acoustic emission (AE) method was introduced so that "when" and "where" of grain crushing might be identified through the interpretation of micro noise that was generated by crushing. Being different from early studies on AE in geotechnical materials, the present study paid attention to the frequency components of the noise and found that noise by grain sliding is of lower frequency while that by crushing exhibits higher frequency. This finding enabled the authors to interpret more accurately the recorded noise, and the timing and location of grain crush during pile penetration were identified. These findings were verified against the independent graphic interpretation of grain movement (PIV). Consequently, a close correlation between AE intensity and yielding of sand were identified. It is important that grain crushing occurs slightly below the elevation of the pile tip and sand immediately below the tip is significantly compressed but less prone to crushing.

KEYWORDS: Pile, Acoustic emission, Crushing, PIV

1. INTRODUCTION

Pile foundation is a common application in modern infrastructure constructions. The design of pile foundation relies on the accurate determination of the bearing capacity of the pile shaft or pile groups. Nevertheless, current design guidelines estimate the ground bearing capacity from either classic plasticity theory or empiricism. The mechanical response of the subsoil and its bearing mechanism are still not well understood. Consequently, the proposed formulations of bearing capacity determination have inevitably been confronted with unreliability, and some of the criteria are even not consistent with the physical processes involved (Randolph et al. 1994). Therefore, there is an ongoing demand to clarify the mechanism of subsoil reactions and the inner interactions between the pile and the surrounding soils (Randolph, 2003).

Establishing the stress and strain conditions developed around the pile tip is crucial to improve the understanding of pile bearing mechanism. In some recent studies, several attempts have been made to investigate the subsoil behavior adjacent to the pile tip.

Jardine et al. (2009, 2013a, 2013b) deployed dozens of soil stress sensors in sand to measure the vertical, radial and circumferential stresses around a closed-ended model pile. It was observed that the stress was concentrated and emanated from the pile tip, and a high-level of stress existed for sand located within ten radii of the pile. Despite a number of sensor used, it should be noted that such measurement was based on point tracing, and consequently further interpolation was required to estimate the stress condition at other positions. In addition, stress concentration may occur due to different rigidity between soil and sensor.

Ekisar et al. (2012) used the X-ray CT to investigate the soil arching on reinforced embankment with rigid pile foundation. White and Bolton (2004) applied the Particle Image Velocimetry (PIV) method to investigate the ground settlement and strain path development in a pile penetration test. These novel methodologies provide direct insights into the subsoil behavior subjected to pile loading. A common observation is that the high level of stress/strain developed around a pile is restrained near ~~to~~ the pile shaft.

It is commonly recognized that particle crushing becomes remarkable in highly stressed soils related to particle crushability, and will eventually affect the mechanical behavior of the materials (Casini et al., 2013). Figure 1 illustrates a typical view of notable sand crushing below a pile tip. The sand immediately below the pile was crushed into white fines. Previous studies evaluated extent of sand crushing using the grain size distribution (GSD) analysis through excavation of sand samples after each test. However, such investigation only gives a general idea of crushing at the end of each test, while the rate of crushing and the accurate locations of the crushing remain unknown.

Figure 1 Significant sand crushing below a pile tip (test at University of Tokyo)

This paper introduces a novel Acoustic Emission (AE) testing method to investigate the subsoil behaviors subjected to vertical pile loading in sand. AE refers to the elastic waves generated by the rapid release of energy in stressed materials (Swindleh, 1973). It concerns with the micro "noises" emitted from the source material. In the theory of plasticity, the plastic straining of a stressed material is accompanied by irrecoverable energy dissipations in forms of heat, vibration and elastic waves (Tanimoto and Tanaka 1986). The elastic waves here, accounting for partial or the total released energies, can be picked by an AE sensor (mostly piezoelectric type) and converted to an electrical signal. In case of pile installation, the sands immediately below the pile tip and around the pile shaft are stressed and the energy is released due to either sand grain sliding or crushing in form of elastic waves. Information carried within these AE signals may provide direct insights to the subsoil response during pile penetration. The major objectives of this study were:

(1) To validate the effectiveness of applying the AE techniques to monitoring of pile loading;
(2) To characterize the process of single pile penetration using AE parameters, and correlate the ground yielding with AE activity;
(3) To investigate the sand crushing behavior using frequency analysis of AE signals;
(4) To visualize the positions of sand crushing using AE source location.

The above objectives are expected to provide certain beneficial references to understand the mechanical features of subsoil under vertical pile loading. Additional image analysis (PIV) and post-test excavations are also performed to verify the AE results.

Furthermore, the proposed AE monitoring method was applied to group pile conditions to investigate the effect of different pile spacing on AE activity.

2. EXPERIMENTAL DETAILS

2.1 Pile loading system

2.1.1 Single pile testing

A series of single pile loading tests were performed to investigate the AE characteristics during pile penetration. All single pile tests presented in this paper were performed in a small pile loading system (Figure 2). The soil tank had a dimension of 600 mm (width) × 600 mm (length) × 500 mm (height). An electrical motor is fixed at the top of metal frame for applying the axial load to the pile. The model pile measured 40mm in diameter, 450 mm in length, and the initial embedment depth was 200 mm. The bearing load of the pile was measured by a load cell, and the settlement was measured by an external displacement transducer. Balloons were installed at the surface to provide realistic surcharge (10 kPa in the current study) to the small model ground. Note that the present test intends to reproduce the situation in subsoil only around the pile tip during penetration.

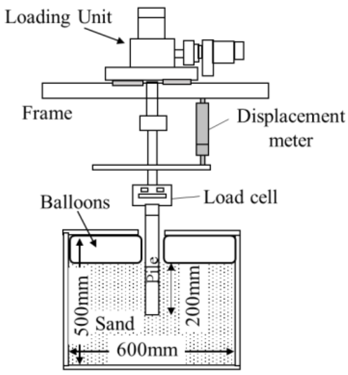

Figure 2 Schematic view of the small pile loading system

The AE testing assembly was further implemented to the pile loading system. Two types of AE sensor arrangement were designed for the purpose of AE activity evolution and AE source location respectively. Figure 3 shows the schematic layout of AE sensor arrangements used in this study. For AE evolution monitoring, sensors manufactured by Fuji Ceramics Corporation, Model R-cast M304A (resonant frequency at 300 kHz), were used. The sensor, with 5.5 mm in diameter and 10 mm in height, was directly attached to the pile surface. Here, the pile shaft, which was made of aluminum, functioned as a wave guide. For AE source location, 8 sensors (Model VS-BV201, manufactured by NEC/TOKIN Corporation) were set around the pile tip aiming to capture a specific signal at the same time. This type of sensor (working frequency: 10Hz-15 kHz) was 11.5 mm in length, 8.5 mm in width and 2.9 mm in height. It is important not to place the sensor too far away from the potential source region. Otherwise the signals may fail to be detected due to attenuation.

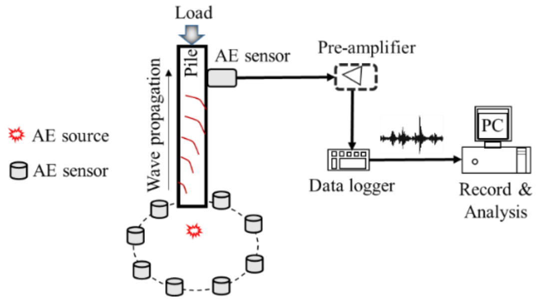

Figure 3 Schematic illustration of AE sensor arrangement

2.1.2 Group pile testing

The AE testing technique was further extended to investigate the group pile behavior. A large pile machine, with inner dimension of 1600 mm (width) × 1600 mm (length) ×1680 mm (height), was employed (Figure 4). The dimension of the large soil tank is approximately three times that of the small one, and consequently, there is less boundary effect on the model ground. The initial embedment depth of pile was set to 550 mm during group pile testing. Air bags were placed on the surface of the model ground in order to simulate a deeper foundation condition, and the surcharge pressure can be adjusted up to 200 kPa. Model piles measured 40 mm in diameter. The group pile model used in this study was constituted of 9 piles (3×3). A rigid steel footing associated with hoop accessories was applied to connect the piles. During group loading, the axial force was applied directly on the footing via a loading head. Two types of pile spacing, 2.5D and 5D, were tested to represent strong and weak group effects.

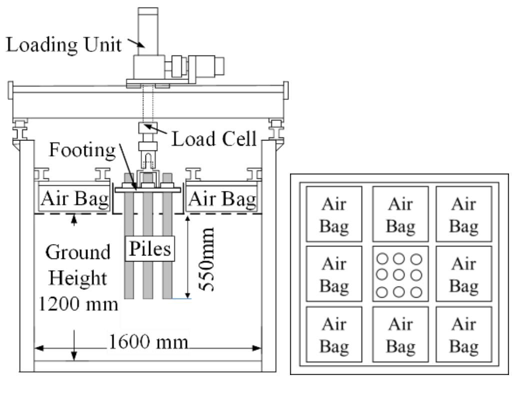

Figure 4 Schematic view of the test apparatus for group pile test: (a) front view and (b) top view

2.1.3 PIV testing

In order to observe the sand grain movement during pile penetration, visualization test based on Particle Image Velocimetry (PIV) measurement was carried out. In this case, the frontal wall of the soil tank was made of a transparent acrylic plate to observe the ground deformation, as shown in Figure 5. Because sand grains around the pile tip move along the surface of the acrylic plate, this series of test may be called pseudo-2D. Because of this 2D condition, additional bracing system was applied to support the pile from the backside. Model ground was prepared by the same method as for the above-mentioned group pile tests. A rectangular parallel pipe made of aluminum, 40 mm × 80 mm in cross section, 4mm thick and 1000 mm length, was used as the 2D model pile. The bottom of the piles was closed by flat plates and the strain gauges were attached inside the pile at the top and bottom. On the surface of pile, which was attached to the acrylic wall, a 7 mm-thick rubber sponge was pasted to fill the gap between piles and the wall. At the tip of a pile, a harder rubber plate with 40 mm × 40 mm in width and 2 mm in thickness, was pasted in place of the rubber sponge.

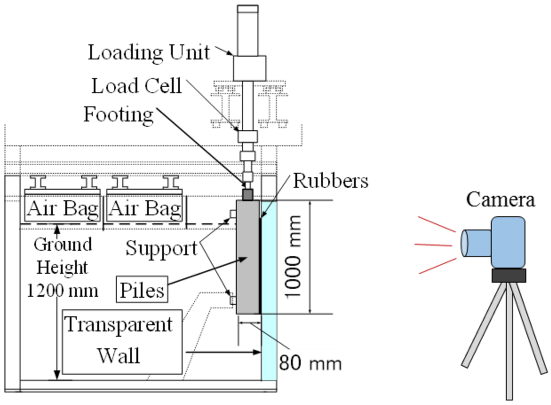

Figure 5 Schematic view of PIV testing

2.2 Tested material

Air-dried silica sand was used as the testing material, with D_{50} = 0.557mm, e_{max} = 1.09 and e_{min} = 0.66. The grain size distribution of the tested material is shown in Figure 6. The model ground was constructed by air pluviation method and manual compaction at every 50 mm (small soil tank) or 150 mm (large soil tank) new deposit to obtain desired relative density.

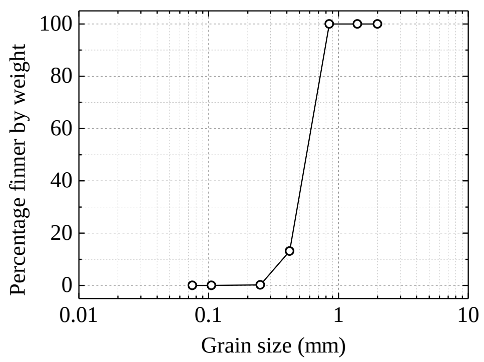

Figure 6 Grain size distribuiton of tested material

2.3 AE parameters

Figure 7 shows a typical AE signal received by the sensor and the AE parameters defined based on it. The AE amplitude represents the peak voltage of the signal wave. The AE energy (E_{MARSE}) is defined by the area under rectified signal envelop (ASM Handbook, 1992). The following equation is therefore used for calculation of the AE energy:

$$E = \frac{1}{2}\sum_{t1}^{t2}\left|V_t \times \Delta t\right| \tag{1}$$

where V is the measured signal voltage, $\triangle t$ is the signal sampling interval. The AE energy rate in this paper represents the amount of cumulated AE energy within every 10s. The time integration in Eq. 1 is divided by 2 for consistency with past studies (Barsoum, 2009; STRP, 2009) which integrated only the positive signals in the time history. The number of event hits are the burst signals with a maximum amplitude crossing a predefined threshold. In addition, the captured signals are converted from the time domain into the frequency domain in order to distinguish two different types of AE events caused by granular sliding or grain crush. The detailed description of this frequency analysis will be discussed next.

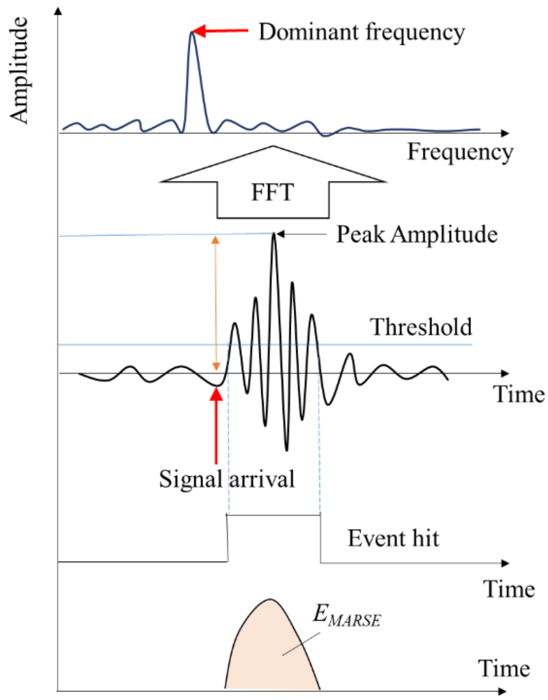

Figure 7 Illustration of an AE signal and relevant parameters

3 Results and discussion

3.1 AE activity during pile penetration

Firstly, model tests were conducted in the small pile loading system to investigate the AE activity during pile penetration. Two types of ground conditions were tested, with relative density (D_r) of 93 % for dense case and 67 % for looser case. Figure 8 (a) illustrates the relationship between the load and settlement during five sequential loadings. It shows that the resistance of dense ground was almost twice as large as loose ground at the same penetration depth. The dependence of the AE characteristics on ground conditions will be discussed next.

Figure 8 (b) and (c) shows the normalized load-settlement relationships of each loading sequence. For both dense and loose test conditions, the tendency of the 1st loading showed notable difference compared with the 2nd-5th loading sequences, where the load increasing period was longer and the increasing rate was much lower.

Figure 9 shows the AE energy development during pile penetration in case of (a) dense ground and (c) looser ground. In general, the released AE energy was relatively low at the beginning of penetration, followed by a rapid increase period and eventually reached certain stable value. For dense case, the AE energy rate during the stable period decreased from the 1st loading to the 5th loading. For loose case, however, it increased from the 1st loading to the 2nd loading sequence. The latter loading sequences showed similar values during the stable period. It is demonstrated that the ground condition could significantly affect the AE characteristics.

Based upon the normalized curves shown in Figure 9 (b) and (d), it is seen that the overall shape and tendency between the load-settlement and AE-settlement curves exhibited high similarity. In addition, the AE-settlement curve of the 1st loading also showed significant difference with the 2nd-5th loading, where the initial rising period of the AE energy during the 1st loading increased much gentler to reach the maximum value compared with the 2nd-5th loading. This is in good consistency with the load-settlement relationships.

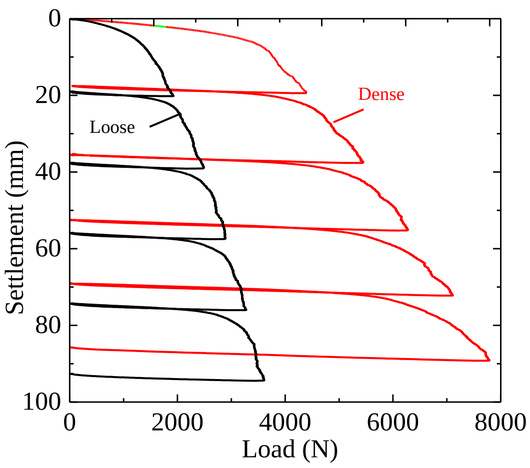

(a)

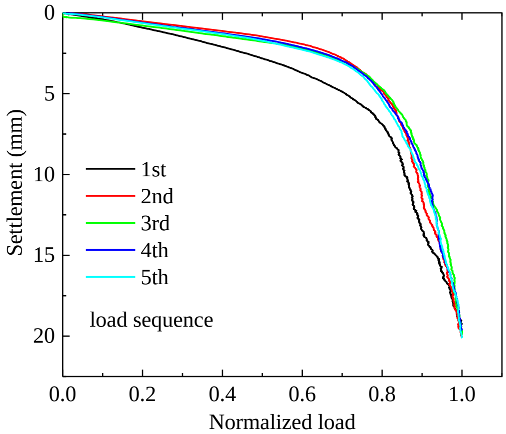

(b)

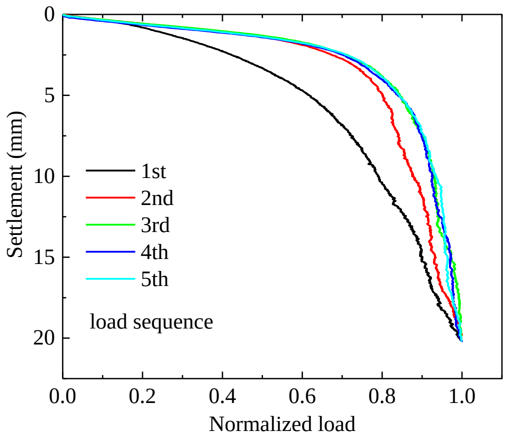

(c)

Figure 8 Load-settlement relationship of single pile tests: (a) measured load-settlement results; (b) dense case: load normalized by the maximum load of each load sequence; (c) loose case: load normalized by the maximum load of each load sequence

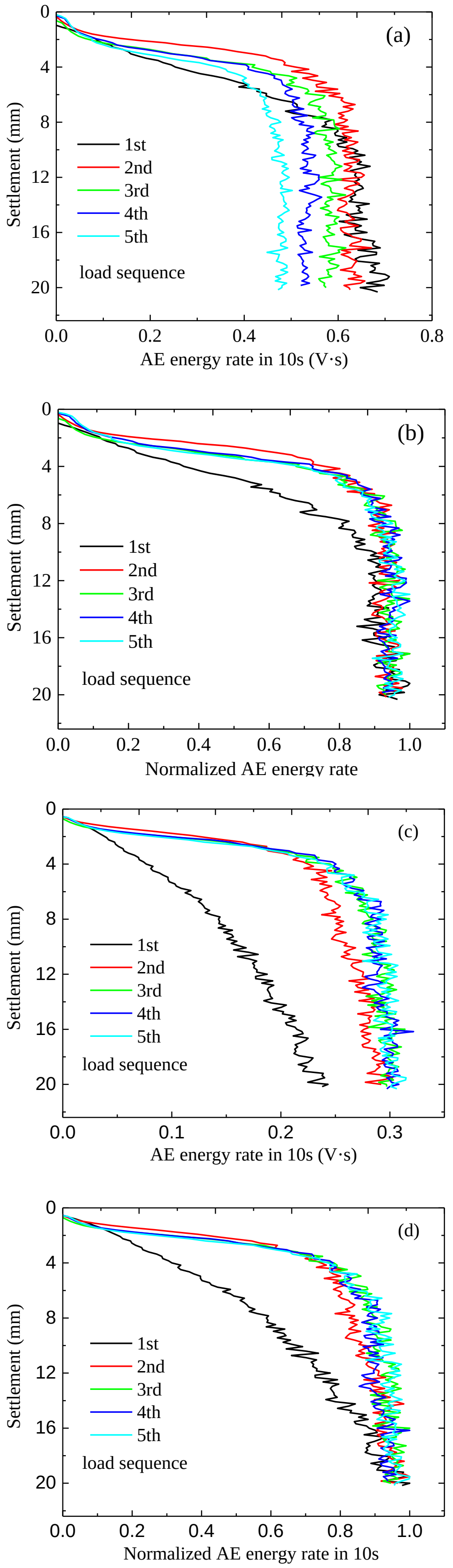

Figure 9 AE energy rate-settlement relationship of single pile tests: (a) dense case: measured AE-settlement results; (b) dense case: AE energy normalized by the maximum AE energy of each load sequence; (c) loose case: measured AE –settlement results; (d) loose case: AE normalized by the maximum AE energy of each load sequence

Figure 10 shows the relationships of load-settlement and AE energy rate (EMARSE) during initial loading and 2nd-loading in case of dense model ground. It is clearly illustrated that the transition period from initial rising to final stabilizing during 1st loading was more gradual than 2nd-loading. The AE activities in the 3rd-5th reloading cycles were found to be similar with the 2nd-loading so that the detailed description was not presented in this paper.

The arrows in Figure 10 indicate the yielding points, which were derived using conventional Casagrande method on load-settlement and AE-settlement respectively. Figure 11 shows the comparison of yield settlements from all five loading steps in dense case. The yield settlements determined by AE showed high consistency compared with those determined by load-settlement relationships. Furthermore, the yield settlements determined by the two methods were even closer during the latter loading sequences than the first loading sequence. It is suggested that the AE method should be potentially useful for evaluating the ground bearing behavior when there are preloading applied on piles, e.g. repeated pile driven during construction process.

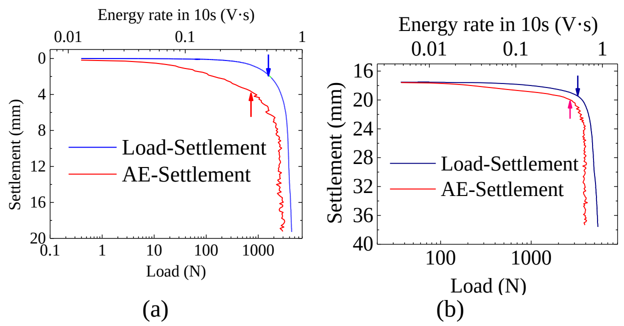

Figure 10 Load-settlement and AE characteristics in case of dense ground for (a) initial loading and (b) 2nd-loading

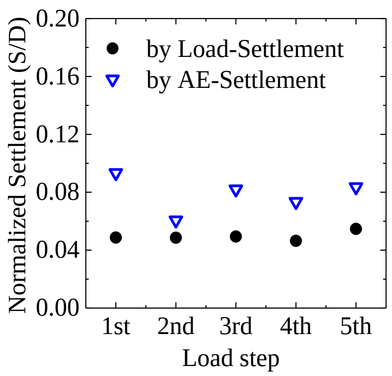

Figure 11 Yield settlement normalized by pile diameter in case of dense ground

3.2 AE signals from crushing and sliding

The detected AE signals from a pile penetration test in sand comes from two main sources: sand grain crushing and sliding. AE technique is particularly helpful when dealing with specific type of mechanical process. Previous studies have shown that AE monitoring technique can be used for failure mode identification (Giordano et al. 1998, Ni and Iwamoto 2002, Gutkin et al. 2011). Among these studies, the dominant frequency of the AE event was often used as the defining parameter for signal differentiation, since it is less affected by testing conditions compared with amplitude or signal duration (De Groot et al. 1995). It is generally recognized that the frequency spectra of a signal is closely related to its source mechanism.

In this paper, two different types of benchmark tests were performed to obtain a general information on the frequency characteristics of the two mechanical processes: sand grain crushing and sliding. Figure 12 illustrates the schematic view of sand sliding and sand crushing tests.

For sand sliding tests, it is important to maintain a low stress level among particles, otherwise the grinding between contacting surfaces may be confused with particle fracturing. Therefore, the test were performed as following: One sand grain was placed on the surface of a metal plate; make the other particle slightly sliding against it; AE sensor was attached on the metal plate to receive~~d~~ generated signals. Figure 13 shows a typical waveform and its spectrum component originating from two particle sliding. The dominant frequency resulting from process was relatively low (52 kHz), and the high frequency component was almost negligible as compared with the dominant frequency. Figure 14 shows the dominant frequency distributions of 150 continuous AE events. It is seen that most of the events have the dominant frequencies less than 100 kHz, with very few exceptions. The most typical range of dominant frequencies is between 4-40 kHz.

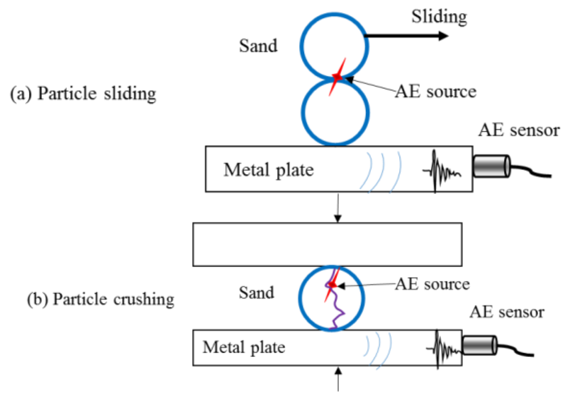

Figure 12 Schematic view of sand sliding and sand crushing tests

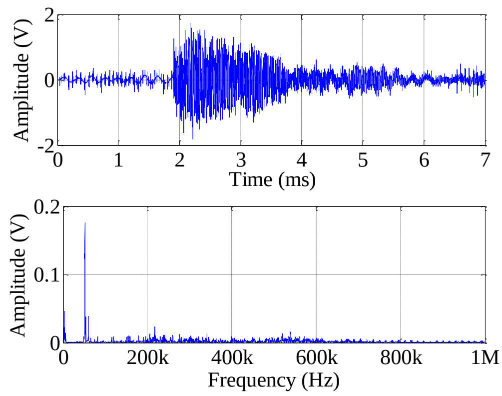

Figure 13 A typical AE signal from sand sliding test and its spectrum component

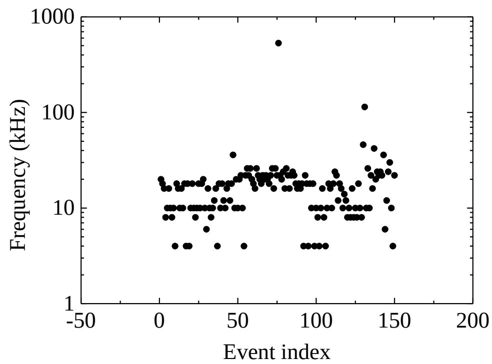

Figure 14 Dominant frequency distribution of 150 continuous AE events from two particle sliding test

For sand crushing tests, single sand grain was placed between two metal plates. The AE sensor was attached on one of the metal plates to detect the released signals. Different from the sand sliding test results, AE signals with high frequency components were substantially observed. Figure 15 shows a typical AE waveform captured from the sand crushing test. It can be seen that the dominant frequency was considerably high (around 137 kHz), while the low frequency components were insignificant.

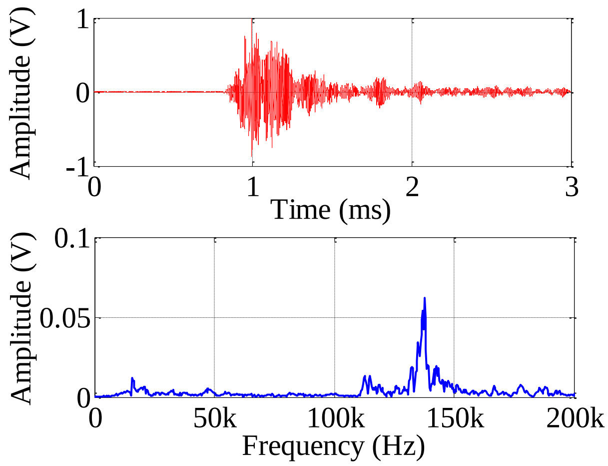

Figure 15 A typical AE signal from sand crushing test and its spectrum component

Figure 16 manifests all captured AE events with high dominant frequency (>100 kHz) during the whole process of single sand grain crushing test. Each hollow circle in the figure represents one AE event. It is noted that the high frequency AEs were mostly observed at high stress level, particularly when there was obvious decrease in bearing load. Considering that high stress level will cause the crack initiation and growth, it is suggested that the high frequency AEs were associated with inner crack development. Therefore, The high frequency components of AE (>100 kHz) can be regarded as a hallmark of the ongoing crushing. Detailed discussions can be found in Mao and Towhata (2015).

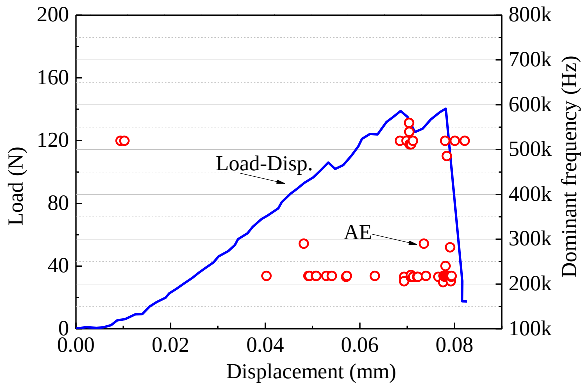

Figure 16 A typical result of dominant frequency (>100 kHz) distributions during particle crushing process (data from Mao and Towhata 2015)

3.3 Sand crushing during pile loading

As discussed above, the significant difference in the frequency content between these two types of events helped to interpret the AE signals recorded during the pile penetration tests. To evaluate the intensity of sand crushing during the process of pile loading, a high-pass filter (>100 kHz) was applied to the AE signals from above mentioned tests to eliminate low frequency signals. The AE signals after the filter were believed to be related with grain fracture source as discussed above.

Figure 17 shows the high-pass AE evolutions with pile penetration in different ground conditions. The overall tendencies are quite similar with those of the total AE, with the absolute magnitude decreased due to the loss of low frequency components. It is demonstrated that the phenomenon of particle crushing accompanied the whole process of pile penetration, although at the very beginning of loading the crushing is not notable. Moreover, the high-pass AE energy in case of dense ground is much higher than that of loose ground. It demonstrated that dense ground will result in more crushing under same penetration depth. Figure 14 also suggests that an almost constant rate of crushing happened after the ground fully yielded. This may be attributed to the well-developed shear surface after ground yielding.

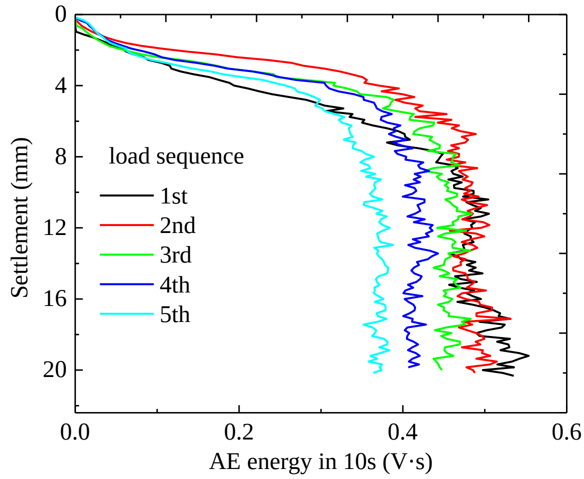

(a)

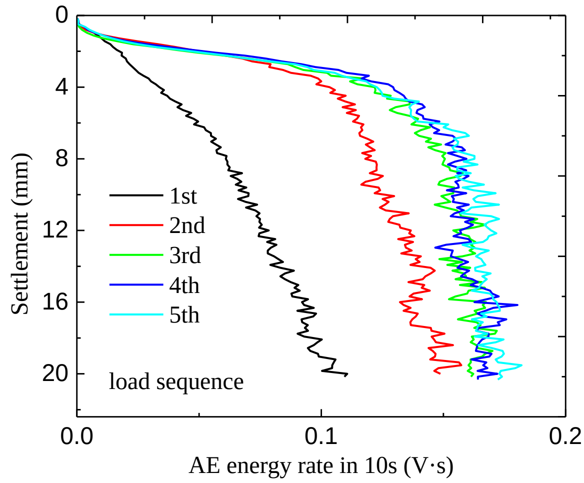

(b)

Figure 17 High-pass AE energy rate during loading processes in case of (a) dense ground and (b) loose ground

Figure 18 shows the ratio of sand crushing and sliding AE counting that change with pile penetration in dense case. Sand crushing represents AE event signals dominated by high frequency, while sand sliding represents AE event signals dominated by low frequency. All curves show that at the very beginning of each loading sequence, the ratio was low and then rose sharply with the process of pile penetration. This observation suggests that the sand crushing was not significant under low stress conditions. Conversely, it occurred substantially when stress was high. Furthermore, the latter loading steps were found to reach the reference line much faster than the previous loading step, indicating that dense ground is more prone to sand crushing.

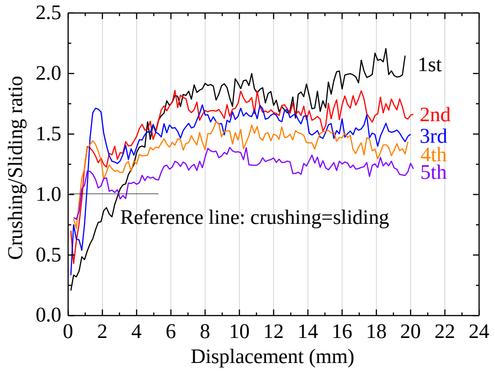

Figure 18 Sand crushing/sand sliding ratio based on numbers of AE event hit

The sands immediately below the pile are heavily compressed, and consequently crushing may easily take place during pile penetration. The significance of sand compaction is illustrated in Figure 19. It can be seen that the sand immediately below the pile tip was substantially compacted from initial thickness of 120 mm (distance between the two color sand layers before pile loading) to 8mm (some sand particles may move out of this layer during pile penetration). In order to evaluate the extent of sand crushing, grain size distribution (GSD) tests were conducted after the pile test. Sand samples were taken from immediately below the pile tip after the test. The results of GSD tests with three sand samples are shown in Figure 20: the original Silica sand, samples after pile penetration in dense and loose ground. It is shown that the fines content of the sand increased greatly after pile penetration, which provides a direct evidence of crushing. In addition, the increment of fines is more significant in case of dense ground, indicating that dense sand is more likely to crush. This result is consistent with AE analysis.

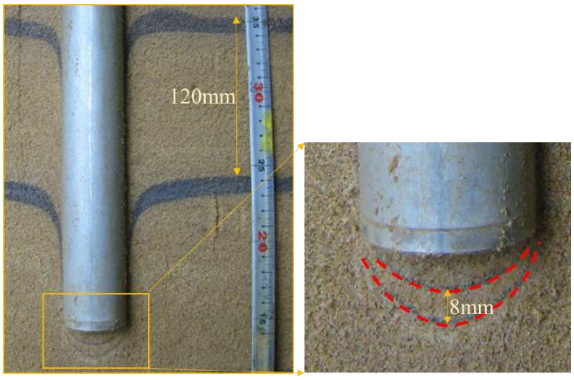

Figure 19 Photo of crushed fines after pile penetration

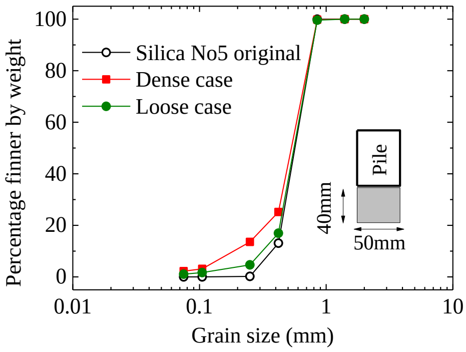

Figure 20 Grain size distributions of sand obtained below pile tip

3.4 AE source location during pile penetration

AE is a part of the irrecoverable energy dissipations due to plastic straining of the stressed material. It is expected that active AE should be associated with locations of severest stress concentration or strain mobilization. The spatial distribution of AE hypocenters provides direct insights into such regions, which is relatively difficult to realize from traditional measurements. Figure 21 is the illustration of transducer arrangement adopted for the AE source localization in this study. The AE transducers were set to surround the target area, i.e. 1-2D depth beneath the pile tip. In a Cartesian coordinate system, the distance (d) between two points, e.g. AE signal source and sensor, can be calculated using the following equation (Miller et al. 2005):

$$d_i = (t_i - t) \times v = \sqrt{(x - x_i)^2 + (y - y_i)^2 + (z - z_i)^2} \tag{2}$$

where t is the real source time, t_i represents the arrival time at i-th transducer, v is the wave velocity which is assumed to be 200m/s based on pre-test measurement, x, y, z are the coordinates of the source and x_i, y_i, z_i are the coordinates of the i-th transducer. In the above equation, only four parameters (x, y, z, t) correlated with AE source are unknown if a constant wave velocity is assumed. Theoretically, a four-sensor array would be able to localize one AE event based on the Time Difference of Arrival (TDOA) among sensors. In practice, more sensors are arranged in order to eliminate the potential errors. In the current study, an eight-sensor array was applied to capture the AE signals around the pile tip. The sensors was buried in sand at designed position as illustrated in Figure 21.

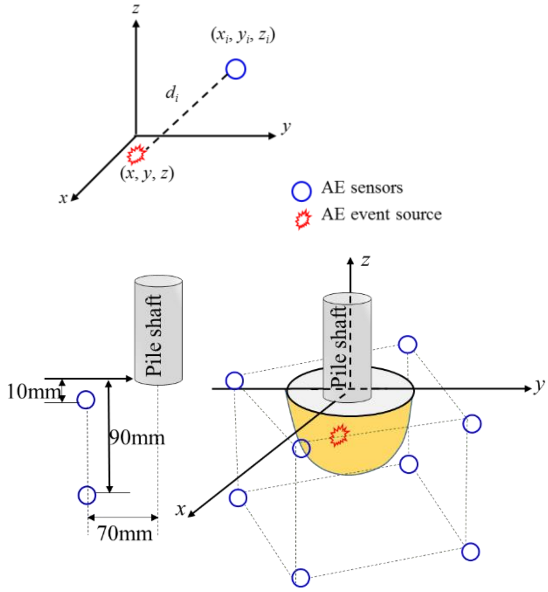

Figure 21 Schematic diagram of sensor array for AE source location

Figure 22 shows the distribution of the localized AE sources at every 2mm pile penetration in terms of pseudo color plotting. A notable feature in Figure 22 is that the AE sources were not uniformly distributed below the pile tip, but concentrated within a limited region about 0.5-1D below pile tip. It is illustrated that the distribution of events was in form of radially extended manner, with density reduced outwards, indicating that the soils within this region underwent severest dislocation or crushing. It is also found that the distance from the location of AE source concentration to the pile tip reduced during pile penetration, suggesting that the subsoil immediately beneath the pile tip was compacted to a certain extent (as illustrated in Figure 19), or was subjected to lateral displacement which resulted in the reduced volume. Detailed discussion will be given in the latter section.

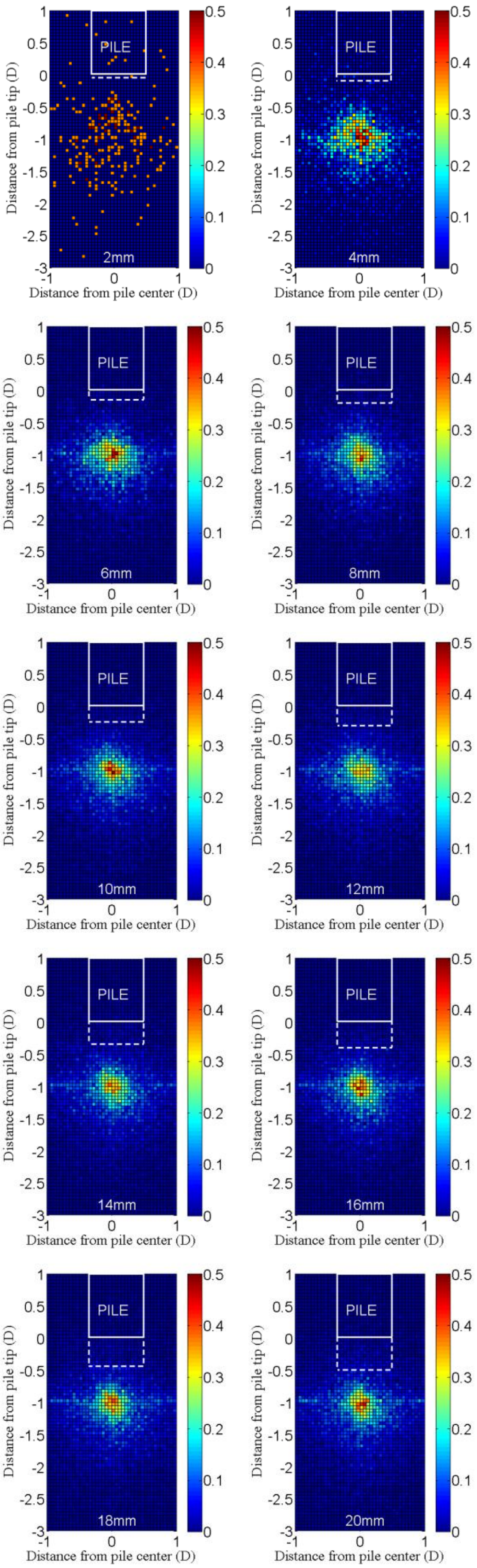

Figure 22 Distribution of AE sources during pile penetration (the color range represents the percentage of AE events occurred within each patch)

Figure 23 shows the number of the localized AE events during every 2mm penetration. The number of localized events at the beginning of loading was much less compared with that in the latter periods. It grew with the penetration and became relatively constant. Such a feature is similar with the evolution tendency of AE activity and the bearing load. It seems that after ground yielding, the AE activity became relatively stable, and therefore the localized AE source number also exhibited same trend.

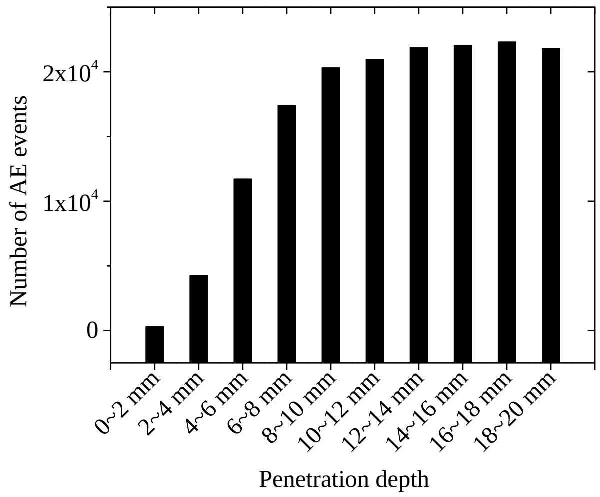

Figure 23 Number of AE events captured at different loading depth

3.5 Zone of sand crushing

From the above AE source location results, AE sources were found to be only concentrated within a limited area. It is indicated that the severest sand crushing may also occurred within the above region. In order to observe the zone of sand crushing, an additional test was conducted with colored and larger grain size sand (same material with silica No.5 but with d_{50}=1.7mm). Figure 24 shows the top view of the ground configuration excavated after 10cm pile penetration. For sand immediately below the pile tip, it appears that there was a circular crushing zone around the pile edge, inside which no obvious crushing can be noticed. The non-crushing region shrunk as the excavation advanced deeper and finally disappeared. Up to 1D depth (40mm), the crushing of sand was insignificant again.

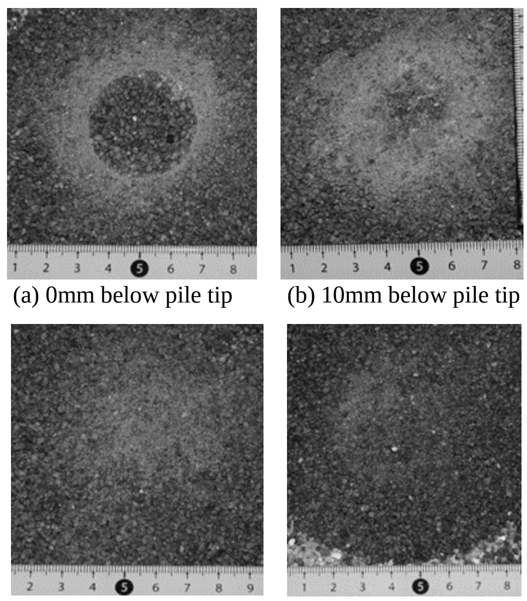

(a) 0mm below pile tip (b) 10mm below pile tip

(c) 30mm below pile tip (d) 43mm below pile tip

Figure 24 Zone of crushing below a flat ended pile tip (light color indicates crushed sand)

White and Bolton (2004) described the crushing zone as the "nose cone" as observed in the calibration chamber test. From the above observation, it is evident that the extent of crushing within the "nose cone" is not uniformly distributed. According to Yang et al. (2010), sand in the shear zone under high normal and shear stress showed high crushing rate. In contrast, sand under high normal stresses without shear banding showed less crushing. It is supposed that sand is more prone to crushed under shear banding than under compression.

The process of a displacement pile installation can be regarded as soil streams passing through a stationary pile (White and Bolton, 2004). In view of sand stream, the crushing of sand below a flat ended pile can be roughly divided into four zones as illustrated in Figure 25: the outer transition zone, the shear band, the inner transition zone and the compression zone. The sand in the shear band underwent severest crushing. The continuous fresh sand flow into the shear band results in substantial crushing with the advancing of pile penetration, and consequently generates considerable AE. The sands localized around the center of the bottom shear zone would change the direction of flow most sharply when entering the shear band below Zone IV in Fig. 25. This region is expected to be most "noisy" in terms of AE, which is consistent with AE source distributions shown above. The observed crushed fines around the edge of pile tip in Figure 24 (a) represents the cumulated crushing during the whole process of pile penetration. The crushed sand previously beneath the central point of pile tip (location where AE source is concentrated) would move laterally towards the pile edge. Therefore, although crushed fines were observed, the AE was insignificant around the pile edge as shown in Figure 22.

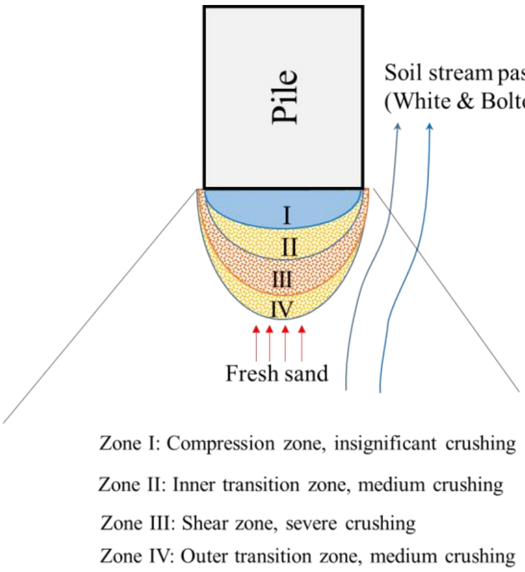

Figure 25 Schematic illustration of sand crushing zone

3.6 Image analysis

The above AE source location results as well as the post-test excavation observations reveal that the extent of sand crushing below a pile tip was different from place to place. In addition, the behavior of the subsoil at about 0.5D~1D below the pile tip seems to be more critical for crushing. In order to have an insight into the inner soil deforming characteristics, the PIV test is conducted to visually observe the ground deformation.

Figure 26 demonstrates a typical results obtained from PIV analysis, which represents the ground deformation pattern after 1mm pile penetration (9-10mm). It can be see that the displacement of the soils is mainly restrained to the pile tip (Figure 26a, b). The soils immediately below the pile tip are "pushed" downward since mainly vertical displacement could be observed. Meanwhile, in the two sides of the pile tip direction, the soils are "pushed" to the two sides of the pile (Figure 26a). Figure 26c shows the shear strain (γ_{xy}) distribution. It is found that the shear strain was mostly developed around pile tip, and the directions of the strain were in opposite side near the pile edge. This confirms the previous assumption that the soils deform (flow) along the pile and change their directions most severely at certain point below pile tip (corresponding to the AE source concentration zone). Consequently, it is reasonable to conclude that the AE is most active at the location where the direction of subsoil "flow" is changed most severely during pile penetration.

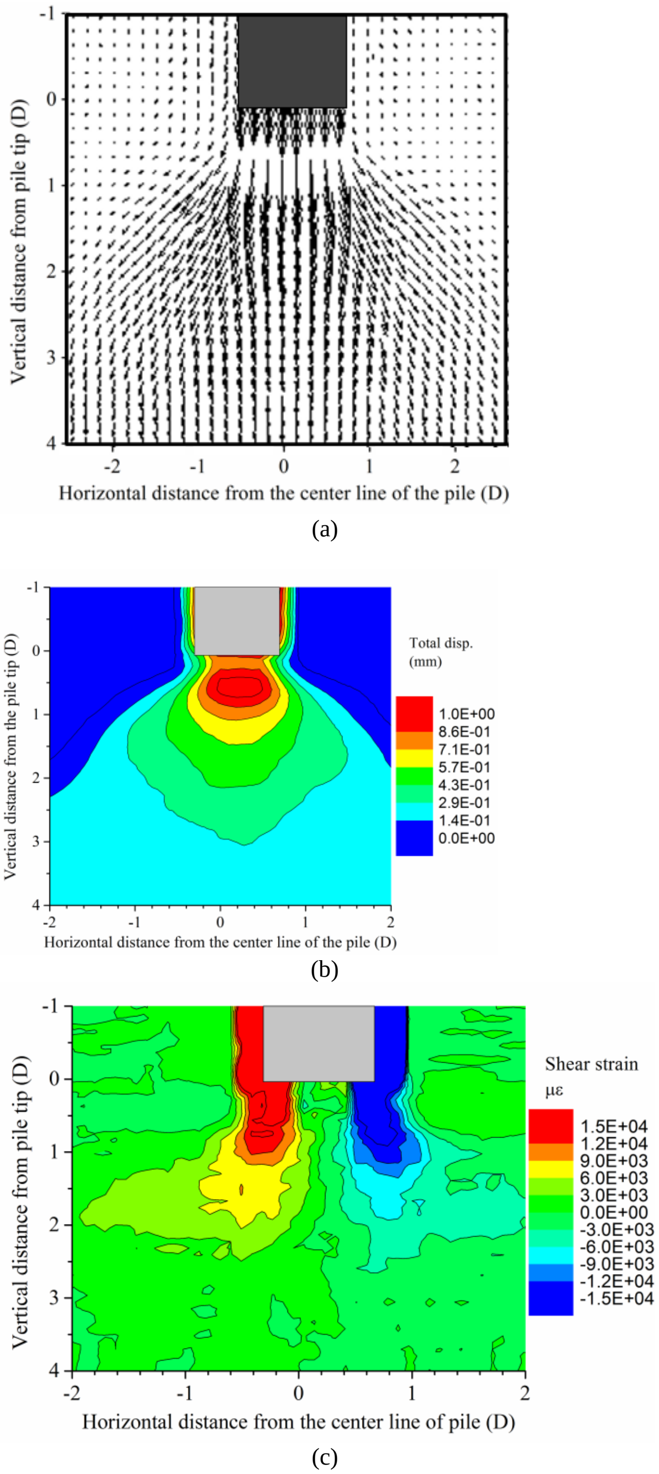

Figure 26 A typical result of (a) displacement field (vector), (b) displacement field (contour) and (c) shear strain field during pile penetration

3.7 Significance of sand crushing on pile bearing capacity

Particle crushing is a common observation in the field of geotechnical engineering. The changed gradation of soils subjected to considerable particle crushing has an essential influence on soil behavior. For example, it is found that particle crushing has significant influence on shear strength, dilatancy, stress path, friction angle and critical state of the tested samples (Lade and Yamamuro, 1996; Hyodo et al., 2002; Sadrekarimi and Olson, 2010; Carrera et al., 2011).

Yu (2014) conducted a series of triaxial tests and found that the peak strengths of the tested sand sample decreased monotonically with increasing particle crushing. As is shown in Figure 27, the peak strength was reduced to about 71 % of the original sand in CD test, and about 55 % in CU test at maximum. Such significance of the strength reduction due to particle crushing should also be considered in pile bearing capacity evaluation.

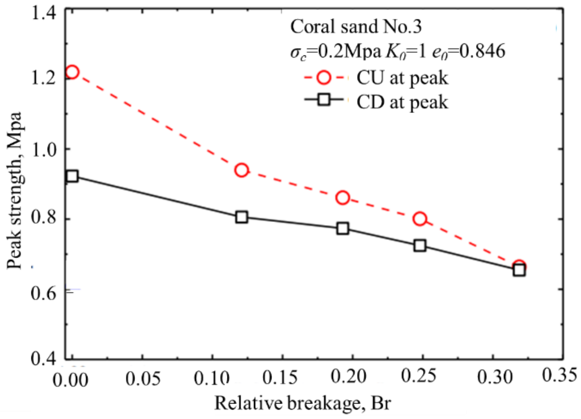

Figure 27 Change of peak strength subjected to particle crushing (breakage) (after Yu 2014)

Kuwajima et al. (2009) performed model pile tests with the soil confined both laterally and vertically. It was found that when the confining pressure increased from 100 kPa to 300 kPa, the bearing capacity of the Toyoura sand increased substantially. In contrast, the bearing capacity of the Dogs Bay sand, a more crushable carbonate sand, failed to increase significantly (Figure 28). This demonstrates the significance of sand crushing on the bearing capacity of piles.

In the previous studies, a reduced rigidity factor which is related with the compressibility of soils is usually used to compute the reduced bearing capacity due to particle crushing (Yasufuku and Hyde 1994, Kuwajima et al. 2009). The compressibility factor obtained from triaxial tests provides an indirect approximation to evaluate the extent of particle crushing.

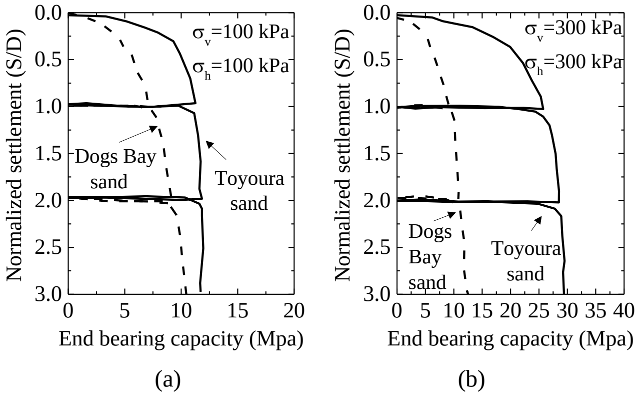

Figure 28 End bearing capacity versus normalized settlement at different confining pressure

Due to the technical difficulty of retrieving crushed fines from time to time during model tests, it is not possible to obtain meaningful correlation between AE and the amount of grain crushing. However, from the current study, it is suggested that the rate of crushing and the geometry of the crushing zone should also be taken into account when formulating the bearing capacity of a pile, which was ignored in most of the previous studies.

3.8 AE monitoring in group pile

Piles are usually used as a group. It is known that bearing behavior of group pile is substantially different from the superposition of the single piles. It was found that there is a certain value of pile spacing at which the mechanism of group failure changes (Whitaker 1957). For those spacing larger than this value, the failure of group pile is analogous with local penetration of individual piles; for those spacing smaller than this value, the failure of group pile occurs together as a block. In case of narrow spacing, the bearing behavior of group pile is substantially different from the superposition of the single piles. The above descriptions have discussed the AE behavior in case of single pile loading.

In this section, the AE testing method is further extended to group pile monitoring. The main objective is to investigate the effect of different pile spacing on the AE activity. Therefore, two type of test conditions, 2.5D and 5D representing narrow pile spacing (strong interaction) and wide pile spacing (weak interaction) respectively, were monitored with AE.

Three piles in the group as well as the loading footing were selected for AE monitoring as shown in Figure 29. The selected three piles represent three different positions corresponding to center, middle and corner piles, respectively. And the sensors were attached near the top of each pile.

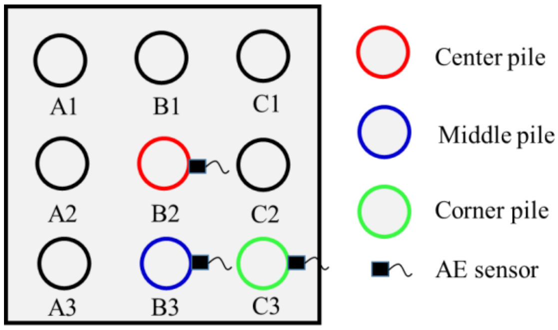

Figure 29 Pile arrangement for AE monitoring

3.8.1 2.5D group pile

Figure 30 shows the results of load-settlement relationship in case of 2.5D group loading. The load here refers to the pile tip resistance measured by strain gauges, which were located at 50 mm above the pile tip. It can be seen that the load-settlement curve of the 1st (initial) loading showed notable difference compared to the reloading steps, especially at the very beginning of penetration. A clear transition point in Figure 30b indicates that ground yielding can be identified from the reloading curve. Another notable point is that the center pile carried more load compared with middle and corner piles. This is attributed to the strong pile-soil-pile interaction in case of narrow pile spacing. This is consistent with the previous study that a narrow pile spacing may significantly reduce the stiffness of the surrounding ground. Meanwhile, the center pile may carry more load than other pile locations due to the induced soil fabric after group pile loading (Aoyama et al. 2016).

Figure 31 shows the AE activity evolution during 2.5D group pile loading. Similar tendencies can be observed compared with the load-settlement curves as shown in Figure 30. The rising of AE in the 1st loading was much slower than the 2nd reloading step. Furthermore, the center pile showed much higher level of AE than the middle and corner piles. Again, the distinct difference between the center pile and the other piles suggested that the AE monitoring can be a useful tool for monitoring of subsoil behaviors.

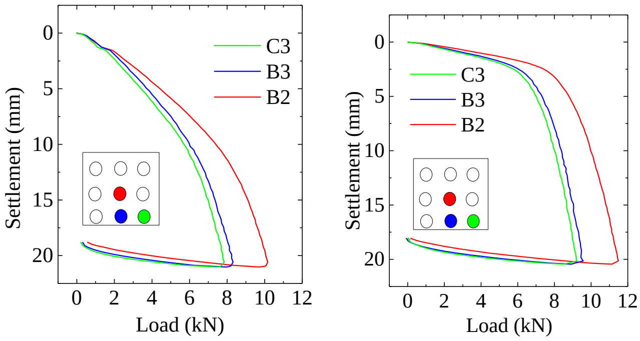

(a) 1st group loading (b) 2nd group loading

Figure 30 Load-settlement relationship during 2.5D group pile

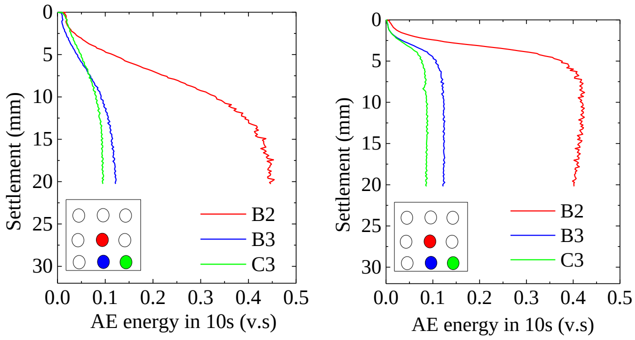

(a) 1st group loading (b) 2nd group loading

Figure 31 AE activity evolution during 2.5D group pile penetration

3.8.2 5D group pile

Figure 32 shows the load-settlement behavior of the piles monitored with AE during 5D group loading. The AE evolution during 5D group pile loading is illustrated in Figure 33. Similar tendencies can be observed compared with the load-settlement curves as shown in Figure 32. Higher tip resistance of piles yielded higher level of AE activity. In Figure 33, the center pile and corner pile showed no obvious difference. It demonstrated that the interaction among piles was insignificant in case of 5D group pile. In such case, the group pile effect could be ignored.

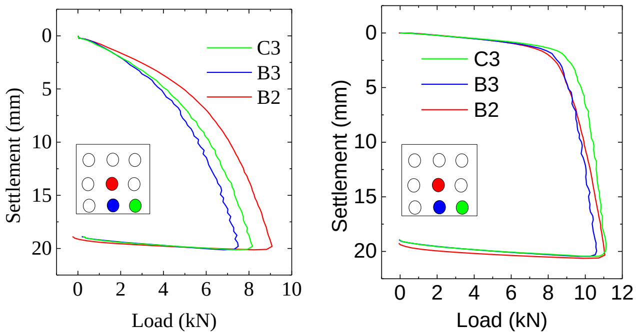

(a) 1st group loading (b) 2nd group loading

Figure 32 Load-settlement behavior during 5D group loading

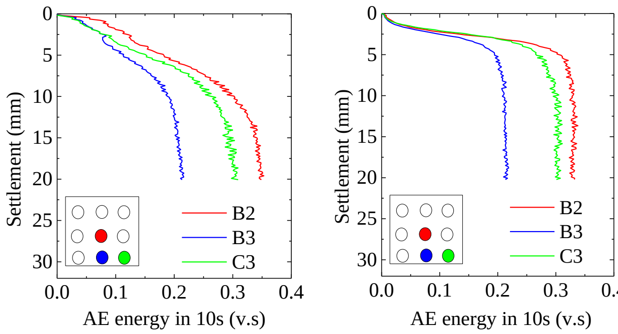

(a) 1st group loading (b) 2nd group loading

Figure 33 AE activity evolution during 5D group pile penetration

Figure 34 shows the evolution of tip resistances of piles at different locations, normalized by the total tip resistance. With 5.0D spacing, the ratio of each pile was almost equal to unity throughout the loading. It suggests that each pile behaved independently. In contrast, for 2.5D spacing, the ratio changed with the penetration of the group pile. The load concentration shifted from the corner piles to the center pile. The corner pile carried more load compared with those of center piles and middle piles at the beginning of group pile loading. This feature was in accordance with the elastic theory of subgrade reaction under rigid foundations (Farouk and Farouk, 2014). The contact stress is minimum at the center and maximum at the edges. This suggests that for 2.5D case, the group pile acted as a whole unit which behaved like rigid foundation, which is correlated with the soil fabric formed due to group pile loading (Aoyama et al. 2016). As pile penetration proceeded, the yielding of soil first initiated near the edge (at corner pile), and consequently the bearing stress of the edge piles ceased to increase substantially, while the central pile was subjected to higher stress at large pile settlement.

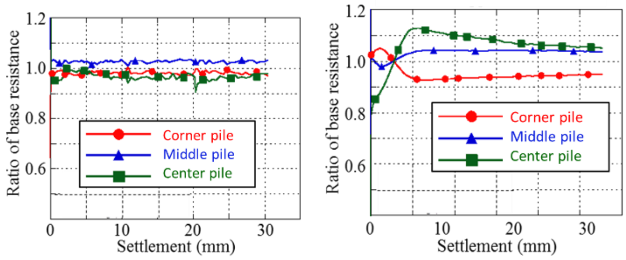

(a) 5D group loading (b) 2.5D group loading

Figure 34 Tip stress distribution in the group pile

4. CONCLUSION

Based on the above discussions, the following conclusions can be drawn:

(1) The process of pile penetration is highly distinguished by AE activities. The evolution tendency of the AE activity showed high similarity with load-settlement curves. Furthermore, the yield settlements obtained from both load and AE data were also close to each other.

(2) The spectra of AE signals originated from the crushing of the particles exhibited a significant rising of high frequency components (>100 kHz). While the AE signals originated from sliding were generally dominated by low frequency components. Significant difference revealed in the frequency content of various AE signals is used for distinguishing sand crushing and sand sliding events.

(3) Sand crushing occurred throughout the pile penetration process, and became significant after the ground yielding. Dense ground was subjected to more crushing. This is evidenced by both AE analysis and GSD analysis.
(4) AE sources were not uniformly distributed below the pile tip, but concentrated within a limited region about 0.5-1D below pile tip. Excavation of subsoil below pile tip after tests showed that the sand crushing mostly occurred in the shear zone. In the compression zone immediately below the pile tip, the crushing was not significant. The lower limit of sand crushing located approximately 1D below the pile tip. This is consistent with AE source concentration results.
(5) The AE testing method was further applied to monitor the group pile tests. The center pile in case of 2.5D group pile showed much higher level of AE activity compared with the corner and middle pile. By contrast in case of 5D group pile, the center pile showed no obvious difference compared with the other piles. This suggests greater interactions between piles in case of narrower pile spacing.
(6) The AE features revealed in this paper provide new insights into the energy dissipation, the extent and the zone of crushing of subsoil subjected to pile load. Potential application of the technique to field pile monitoring is also promising.

5. ACKNOWLEDGEMENT

PIV program used in this study was provided by Prof. David J. White of University of Western Australia. Financial supports were provided by Dr. S. Yabu-uchi. These assistances are greatly acknowledged by the authors.

6. REFERENCES

Aoyama, S., Mao, W., Goto, S., and Towhata, I. (2016). Application of Advanced Procedures to Model Tests on the Subsoil Behavior Under Vertical Loading of Group Pile in Sand. Indian Geotechnical Journal, 46(1), 64-76.

ASM Handbook: Nondestructive Evaluation and Quality Control, 1992, ASM International, Vol.17, 9th edition. 593-682.

Barsoum F.F., Soleman J., Korcak A. and Hill E.V.K. (2009) Acoustic emission monitoring and fatigue life prediction in axially loaded notched steel specimens, Journal of Acoustic Emission, 27: 40-63.

Carrera A.W., Coop M.R. and Lancellotta R. (2011) The influence of grading on the mechanical behaviour of stava tailings. Geotechnique, 61(11):935-946.

Casini, F., Viggiani, G.M.B. and Springman, S.M. (2013) Breakage of an artificial crushable material under loading. Granular matter. 15(5):661-673.

Dagois-Bohy, S., Ngo, S., Pont, S. C. D., and Douady, S. (2010) Laboratory singing sand avalanches. Ultrasonics, 50(2):127-132.

De Groot, P. J., Wijnen, P. A., and Janssen, R. B. (1995) Real-time frequency determination of acoustic emission for different fracture mechanisms in carbon/epoxy composites. Composites Science and Technology, 55(4), 405-412.

Ekisar, T., Otani, J., and Hironaka, J. (2012) Visualization of soil arching on reinforced embankment with rigid pile foundation using X-ray CT. Geotextiles and Geomembranes. 32:44-54.

Farouk, H. and Farouk, M. (2014) Effect of Footing Rigidity on Contact Stress. Recent Advances in Material, Analysis, Monitoring, and Evaluation in Foundation and Bridge Engineering. 78-85.

Giordano, M., Calabro, A., Esposito, C., D'amore, A., and Nicolais, L. (1998). An acoustic-emission characterization of the failure modes in polymer-composite materials. Composites Science and Technology, 58(12), 1923-1928.

Gutkin, R., Green, C. J., Vangrattanachai, S., Pinho, S. T., Robinson, P., and Curtis, P. T. (2011) On acoustic emission for failure investigation in CFRP: Pattern recognition and peak frequency analyses. Mechanical Systems and Signal Processing, 25(4), 1393-1407.

Hyodo, M., Hyde Adrian F.L., Aramaki N., and Nakata Y. (2002) Undrained monotonic and cyclic shear behavior of sand under low and high confining stresses. Soils and Foundations, 42(3):63-76.

Jardine, R. J., Zhu, B., Foray, P., and Dalton, C. P. (2009) Experimental arrangements for investigation of soil stresses developed around a displacement pile. Soils and Foundations, 49(5), 661-673.

Jardine, R. J., Zhu, B. T., Foray, P., and Yang, Z. X. (2013a) Interpretation of stress measurements made around closed-ended displacement piles in sand. Géotechnique, 63(8), 613-627.

Jardine, R. J., Zhu, B., Foray, P., and Yang, Z. X. (2013b) Measurement of stresses around closed-ended displacement piles in sand. Geotechnique, 63(1), 1-17.

Kuwajima, K., Hyodo, M., and Hyde, A. F. (2009). Pile bearing capacity factors and soil crushabiity. J Geotech Geoenviron, 135(7): 901-913.

Lade, P. V., Yamamuro, J. A., and Bopp, P. A. (1996) Significance of particle crushing in granular materials. Journal of Geotechnical Engineering, 122(4): 309-316.

Mao, W., and Towhata, I. (2015) Monitoring of single-particle fragmentation process under static loading using acoustic emission. Applied Acoustics, 94, 39-45.

Miller, R. K.,. Hill, E. v. K., Moore, P. O. (2005) Nondestructive Testing Handbook, Third Edition: Volume 6, Acoustic Emission Testing, America Society for Nondestructive.

Ni, Q. Q., and Iwamoto, M. (2002) Wavelet transform of acoustic emission signals in failure of model composites. Engineering Fracture Mechanics, 69(6), 717-728.

Randolph, M. F. (2003). Science and empiricism in pile foundation design. Geotechnique, 53(10), 847-875.

Randolph,M. F., Dolwin, R., and Beck, R. (1994). Design of driven piles in sand. Geotechnique, 44(3), 427-448.

Sadrekarimi A. and Olson S.M. (2010). Particle damage observed in ring shear tests on sands. Canadian Geotechnical Journal, 47(5): 497-515.

Strategic Targeted Research Project (STRP) (2009) D08: Recommendations on the use of results of monitoring on bridge safety assessment and maintenance, Annex C: The Acoustic Emission Method, Report on ARCHES Assessment and Rehabilitation of Central European Highway Structures.

Swindleh, W. (1973). Acoustic emission. 1. Introduction. Non-destructive testing. 6(3):152-158.

Tanimoto, K., and Tanaka, Y. (1986). Yielding of soil as determined by acoustic emission. Soils and foundations, 26(3), 69-80.

Whitaker, T. (1957). Experiments with Model Piles in Groups*. Geotechnique, 7(4), 147-167.

White, D. J., and Bolton, M. D. (2004). Displacement and strain paths during plane-strain model pile installation in sand. Géotechnique, 54(6), 375-397.

Yasufuku, N. and Hyde, A.F. (1995) Pile end bearing capacity in crushable sand. Geotechnique 45(4), 663-676.

Yang, Z. X., Jardine, R. J., Zhu, B. T., Foray, P., and Tsuha, C. H. C. (2010). Sand grain crushing and interface shearing during displacement pile installation in sand. Géotechnique, 60(6), 469-482.

Yu F.W. (2014) Experimental study on particle breakage under high pressure. Doctoral dissertation, University of Tokyo, Tokyo.